Chemical Physics Letters 512 (2011) 54–59

Contents lists available at ScienceDirect

Chemical Physics Letters

journal homepage: www.elsevier.com/locate/cplett

Ab initio modeling of fused silica, crystal quartz, and water Raman spectra

Martin Dračínský *, Ladislav Benda, Petr Bouř *

Institute of Organic Chemistry and Biochemistry, Academy of Sciences, Flemingovo nám. 2, 16610 Prague 6, Czech Republic

ARTICLE INFO

Article history:
Received 15 April 2011
In final form 27 June 2011
Available online 30 June 2011

ABSTRACT

Fused silica light-scattering properties are important for many industrial and laboratory applications. In this work, ab initio molecular dynamics employing periodic boundary conditions are used to simulate its structure and Raman scattering. Fused silica geometry is modeled as a frozen liquid, and the spectra are compared to those of crystal quartz. The method is tested also on Raman spectra of liquid water. Structural similarities between water and fused silica are discussed. The modeling agrees with experiment and suggests that most fused silica spectral features can be explained within the harmonic approximation. The combination of Raman spectroscopy with theoretical computations thus appears useful for structural studies of amorphous materials.

1. Introduction

Fused silica is commonly used synthetic form of the silicon dioxide (SiO_2). It is manufactured from crystal quartz that melts at above 1700 °C. It has superior thermal, mechanical, chemical, and optical properties if compared to other glasses. A silica thread is often used in optical fibers [1].

Both infrared light in the absorption spectroscopy [2] and visible radiation in the Raman-scattering [3] can be used to probe the fused silica vibrational properties. Indeed, these spectroscopic techniques are often used to study its structure and reactivity. For example, Raman microscopy was proposed for a surface damage monitoring [4], the silica substrate was used for surface enhanced Raman spectroscopy SERS [5], and sol–gel silicate glasses were studied by IR and Raman scattering [6].

We found a particular need to understand the origin and position of fused silica Raman bands in Raman optical activity (ROA) experiments, where the fused silica cells are used to hold the sample. The ROA method measures tiny differences in scattering of left and right circularly polarized light. However, if the sample signal is weak, it interferes with the scattering from the cell windows [7]. Even in unpolarized Raman experiments, where the lowest-frequency region is needed, such as those employing weak metal complexes [8], the sample signal needs to be carefully separated from a baseline including the fused silica signal.

Previously, rather empirical approaches were used for fused silica spectral analyses. For example, several components were identified in the fused silica Raman spectrum, although they were not assigned to the structure [9]. Molecular dynamics (MD) and a fixed partial charge model were used to model vibrations of SiO_2 surfaces [10]. Vibrations in SiO were found similar to those in SiO_2, and could be modeled with a Brendel-type dielectric function [11]. When an interaction-induced phonon Raman scattering was modeled phenomenologically and related to the structure, an interesting analogy to the water scattering properties was observed [12]. High-pressure experiments revealed notable Raman intensity changes that were assigned to an intermediate-range order in fused silica [3]. All these results suggest that the Raman spectra bear interesting information about the structure that can be eventually deciphered by the simulations.

Within the central force network model, the fused silica experimental spectra could have been interpreted in terms of empirical force constants and geometry parameters. The model assumes a relatively regular tetrahedral structure, although it allows for a force constant correction dependent also on the bond angle. In spite of the crude approximation, it explained most important SiO_2 spectral features, and enabled comparison to similar tetrahedral glasses (GeO_2, BeF_2) [13]. Ab initio molecular dynamics with the periodic boundary conditions provided realistic Raman intensities for the silicate crystal [14]. To the best of our knowledge, however, a priori model of the fused silica Raman spectral response does not exist.

In this work, we used the Car–Parrinello molecular dynamics (CPMD) [15] to model the fused silica structure as a frozen liquid. Thanks to the extension of the coupled-perturbed techniques for infinite periodic systems [16] the harmonic vibrational frequencies and Raman scattering intensities could be calculated quantum mechanically within the GGA DFT approximation [17]. Optimal computational parameters were determined for the spectrum of quartz crystal, where the vibrational frequencies were better resolved than in the fused silica.

Alternate usage of conventional MD is currently not possible for the fused silica; a reliable force field for melted SiO_2 is not known

* Corresponding authors.
E-mail addresses: dracinsky@uochb.cas.cz (M. Dračínský), ladislav.benda@uochb.cas.cz (L. Benda), bour@uochb.cas.cz (P. Bouř).

0009-2614/$ - see front matter © 2011 Elsevier B.V. All rights reserved.
doi:10.1016/j.cplett.2011.06.077

to us. The force field would have to allow for Si—O bond creation and breaking needed to equilibrate the 'frozen' fused silica geometry. This is, on the other hand, automatically involved in CPMD.

A liquid water CPMD simulation was also performed, to test the method, but also to point out structural similarities and differences to fused silica. For fused silica, the method provides larger inhomogeneous broadening of Raman spectral lines when compared to another form of SiO_2, the crystal quartz, and indicates that the Raman spectra are sensitive to the structure, which can be potentially used for probing similar materials.

2. Method

Experimental spectra of a natural quartz crystal and fused silica window of a standard spectroscopic cell (JASCO 120-QS) were obtained with the Biotools Raman instrument. The experimental conditions were as follows: laser wavelength 532 nm, laser power at the sample ~20 mW, spectral resolution ~10 cm^{-1}, acquisition times ~5 min. Backscattered Raman spectrum of water was obtained on a spectrometer located at the Physical Institute of the Charles University, at 300 K and in a broader 50–4000 cm^{-1} wavenumber range.

Crystal quartz Raman spectra were simulated based on the experimentally determined [18] cell parameters (298 K, AMC structure database code 0006362). With CASTEP [19,20] the geometry parameters were optimized using the PBE [21] functional and Raman intensities were calculated numerically at several levels (Table 1). The geometries were optimized and vibrational frequencies were calculated also using the Quickstep module [22] of the CP2K program (http://cp2k.berlios.de/) with the BLYP functional [23], the Gaussian and plane waves DZVP basis set [24], and the GTH norm-conserving pseudo-potentials [25]. Note that the Raman intensities are not implemented in CP2K.

The initial geometry of fused silica (SiO_2 glass phase) was taken from an MD simulation of water, where the oxygen and hydrogen atoms were replaced by silicon and oxygen atoms, respectively. Then a Car–Parrinello molecular dynamics (CPMD) [15] was run using the *NVT* ensemble and 10.419 Å cubic periodic box (75 atoms), within the CPMD software [26]. To maintain numerical stability during the initial equilibration, 18 short simulations (200 steps each) were performed while gradually increasing the temperature (500 → 2200 K) and integration time step (0.048 → 0.14514 fs). After each simulation, the wavefunction was reoptimized to quench the system to the Born–Oppenheimer surface. With 0.14514 fs integration time step a longer 40 ps (about two months of CPU E7330/2.40 GHz time) equilibration run was performed. Finally, four geometries for the spectral simulations were selected at 5, 10.8, 16.4 and 22.4 ps of a production run. Similarly as for the quartz, the CPMD snapshot geometries were optimized using the CASTEP software, and the harmonic force field and Raman intensities were calculated by the default numerical differentiation. For the fused silica, our own scripts were used to generate radial and angular distribution functions.

For comparison, a CPMD simulation of liquid water described previously [8] (0.097 fs time step, NVT ensemble, 300 K, 9.957 Å box, total time of 6.6 ps) was used to generate geometry distribution and snapshots (22 clusters taken each 0.3 ps) for the spectral computations. These geometries were optimized and subjected to calculation of vibrational frequencies within the CP2K program using the method described above. The polarizability derivatives needed for the Raman intensities were calculated by the Gaussian program without the periodic boundary conditions. Water, unlike the fused silica, is composed of well-defined molecules. Therefore the neglect of the periodic box boundary interactions had only minor effect on the spectra. The Gaussian program enabled us to use a presumably more precise hybrid functional (B3LYP) [27] than CASTEP relying on GGA functionals only. Also the basis set size could be varied more extensively.

To estimate the influence of more delocalized longer-range modes in fused silica, we propagated the elementary cell geometry

Table 1
Quartz crystal calculated and experimental frequencies (cm^{-1}) at several approximation levels.

	CP2K	CAS1	CAS2	CAS3	CAS4	CAS5	CAS6	CAS7	CAS8	
Functional	BLYP	PBE	PBE	PBE	PBE	PBE	PBE	PW91	LDA	
E_{cutoff} [eV]	3810	500	330	330	450	550	550	500	500	
k-point set	–	3 × 3 × 4	2 × 2 × 2	2 × 2 × 2	3 × 3 × 2	3 × 3 × 4	3 × 3 × 4	3 × 3 × 4	3 × 3 × 4	
SCF toler. [eV/atom]	10^{-5}	10^{-6}	10^{-5}	10^{-5}	2×10^{-6}	5×10^{-7}	5×10^{-7}	10^{-6}	10^{-6}	
Converg.[a] [Å^3]	–	10^{-5}	10^{-5}	10^{-4}	10^{-5}	10^{-5}	10^{-6}	10^{-5}	10^{-5}	
CPU time [h]	8.8	10	1.5	1.4	6.5	19	25	13	10	
Mode[b]										Exp.
1 2c	1087	1198	1219	1220	1204	1197	1197	1213	1181	1163
2 1c	1041	1116	1163	1163	1120	1116	1115	1131	1111	1067
3 1b	*982*	*1105*	*1152*	*1153*	*1107*	*1105*	*1105*	*1120*	*1101*	
4 2a	1002	1099	1143	1144	1102	1099	1099	1113	1094	1047
5 2a	788	784	804	804	783	784	784	787	779	807
6 1b	*730*	*783*	*803*	*804*	*782*	*783*	*783*	*786*	*774*	
7 2a	676	683	691	691	684	683	683	689	676	698
8 1b	*516*	*454*	*426*	*426*	*454*	*454*	*454*	*464*	*441*	
9 1c	557	435	418	418	438	436	436	441	421	465
10 2a	538	425	379	378	431	425	425	435	408	
11 2a	446	391	332	332	397	390	390	407	372	400
12 1b	*467*	*380*	*362*	*362*	*388*	*380*	*380*	*393*	*356*	
13 1c	457	355	319	318	359	355	355	363	338	354
14 2a	413	246	217	217	248	249	249	256	237	262
15 1c	266	109	i138[c]	i138[c]	115	109	109	166	132	206
16 2a	326	104	i143[c]	i143[c]	117	106	106	160	107	
δ_{RMS}	75	42	86	86	42	42	42	37	38	0

[a] Convergence required for the second-order response to the electric field in the Raman spectra calculation.
[b] Symmetry and degeneracy are indicated, the *b* modes (italics, shaded) are not Raman active, *c* modes are IR-forbidden (point group 19, D3).
[c] Imaginary frequencies.

along the Cartesian axes to cubes containing 75, 600, 2025 and 4800 atoms (corresponding to the original cell and its $2 \times 2 \times 2$, $3 \times 3 \times 3$, and $4 \times 4 \times 4$ multiples, respectively). Note that within the periodic boundary conditions, the cell is well defined also for amorphous materials. The force field and polarizability derivatives were transferred [28] from the elementary cell as obtained by CASTEP. The Cartesian energy and polarizability derivatives were obtained by a linear transformation from the normal mode cell parameters and the Cartesian-normal mode transformation matrix, also provided by CASTEP. The Raman spectra were calculated by the Fourier transform (FT) method based on a propagation in arbitrary time [29]. The FT approach is faster than a full diagonalization, and allows obtaining spectra of very large systems. Ten propagation vectors [29] were averaged during the FT propagation.

To qualitatively analyze the fused silica vibration, distance, valence and torsion angle coordinates were introduced for the first CPMD snapshot geometry (75 atoms), so that intrinsic potential energy distribution (PED) could be calculated using the CASTEP harmonic force field. For the smaller crystal quartz cell (9 atoms), the introduction of the internal coordinates implying projection of rotational degrees of freedom led to larger frequency errors; thus a classification of the normal modes based on the crystal symmetry was preferred in this case (Table 1).

From the calculated Raman intensities, all spectra were generated with Lorentzian profiles 10 cm^{-1} wide (full width at the half height); the glass spectrum was slightly smoothed by a convolution with a 10 cm^{-1} wide Gauss function.

3. Results and discussion

3.1. Distribution functions of fused silica and water

In spite of the obvious differences, there are some amazing analogies between the liquid water and fused silica structure and behavior. In both systems, the bond network is based on approximately tetrahedral central atom (Si for silicon, O for water) and a monatomic bent link (–O– and –H. . .). The pyramidal arrangement also stabilizes the ordered states, i.e. the ice for water and quartz for fused silica. However, material density increases for quartz (to 2.65 g/ml, from 2.201 g/ml of silica, i.e. by ~17%), whereas the ice density (0.9167 g/cm^3) is smaller than that of water at 0 °C (0.9998 g/cm^3, i.e. by ~8%) [30].

The structural similarities are reflected in the calculated angular distribution functions (Figure 1, top). The O–Si–O angle band is centered around 107°, which very well corresponds to the exact value of ~109° of the sp^3 hybridization, and thus also provides feedback on the convergence of the calculations. In the water structure, the calculated most probable value of the H–O–H angle of 106° (Figure 1, top right) only slightly deviates from the ideal case of 104.5° due to the lone electron pair repulsion. However, the aqueous distribution is broader (~from 60° to 170°) than that of the silica (~80°–130°), which reflects the fact that all bonds in the latter system are covalent. The Si–O–Si link angular distribution is relatively broad (~100°–180°) and also well corresponds to the experiment (120°–180°) [31]. It is centered around 134° (a value of 144° was estimated by X-ray diffraction [31]), while the hydrogen bond network in water provides the most probable O–H..O angle of 166°.

The calculated most probable Si–O distance (1.65 Å, Figure 1, bottom left) is in agreement with the distance of 1.62 Å found experimentally [31], and confirms the equivalence of all four Si—O bonds that were predominantly present at each Si atom during the simulation. The radial distribution function in water is, however, quite different (Figure 1, bottom right), with two peaks corresponding to the covalent (~0.99 Å) and non-covalent (~1.83 Å) OH bonds.

3.2. Quartz vibrational frequencies

The crystal quartz was used to test the precision of calculated vibrational harmonic frequencies. The results calculated for the $\Gamma(0, 0, 0)$ phonon branch (i.e. including only the vibrations within the 75 atom periodic cell) are listed in Table 1. Within the applied computational parameters, the agreement of calculated vibrational frequencies with experiment is poorer for the CP2K program (RMS frequency error $\delta = 75$ cm^{-1}) than for CASTEP (42 cm^{-1}), although both approaches provide realistic ordering of the vibrational transitions (Table 1). Relaxing the energy cutoff used to restrain the plane wave basis in CASTEP and the *k*-space point set significantly shortens the computational time (10 → 1.4 h), but the RMS deviation doubles, and the two lowest frequency modes (number 15 and 16) are produced with negative (imaginary) frequencies. On the other hand, increasing the SCF tolerance (the CAS5 and CAS7 computations, Table 1) approximately doubles the computational time

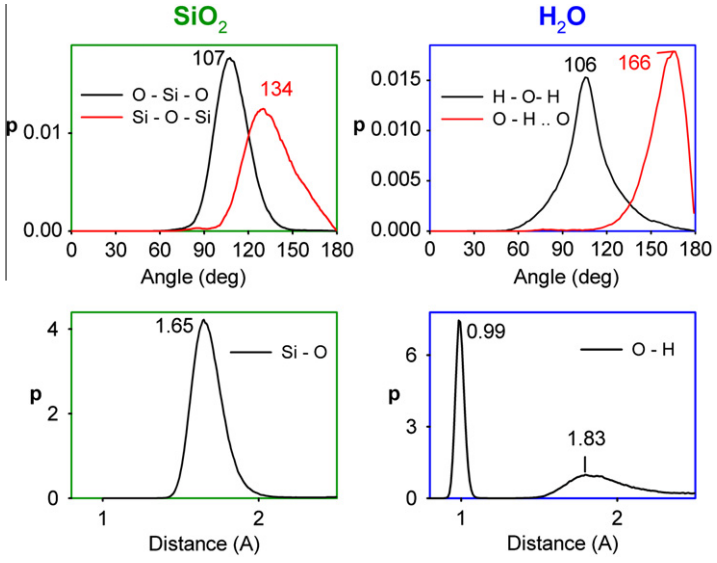

Figure 1. Comparison of the liquid SiO_2 (left) and water (right) angular (top) and radial distribution functions (bottom) obtained from the CPMD simulation.

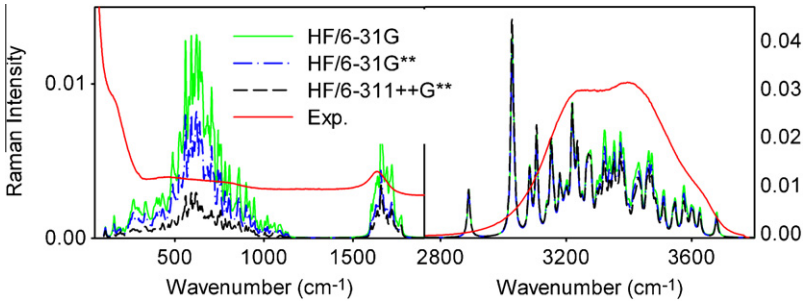

Figure 2. Raman intensities of water simulated with CP2K frequencies for a randomly chosen CPMD cluster with the polarizability derivatives calculated with three basis sets, and the experimental spectrum. The experimental intensity scale is arbitrary. Note that cell window signal significantly distorts the experimental scattering below 250 cm^{-1}.

without any significant influence on the results. The PW91 [32] and LDA functionals (CAS7 and CAS8 approximations, respectively) provide nearly the same frequencies as the default PBE functional within approximately the same time. Raman intensities obtained by the eight CASTEP computations (not shown) were quite similar. Thus we can conclude that the computed vibrational properties of crystalline quartz are relatively independent of the DFT functional and SCF convergence criteria; on the other hand, it is difficult to reduce the computational demands without a significant loss of accuracy.

3.3. Basis set dependence of the lowest-frequency vibrations in water

For the water box, a more extensive exploration of basis set dependence could be done than for SiO_2. For water the CP2K vibrational frequencies (normal mode) could be combined with the polarizability derivatives obtained by GAUSSIAN. The Raman intensities at the Hartree–Fock level are presented (Figure 2) as they are nearly the same as those obtained with the B3LYP and BPW91 functionals (not shown). We found interesting the comparison of the 6-31G, 6-31G** and 6-311++G** results plotted in Figure 2, as it documents a rather different character of the lower-frequency vibrations. Clearly, the lowest-frequency modes involving water molecule translations and rotations are more sensitive to the basis set size, whereas the H–O–H bending (~1650 cm^{-1}) and O–H stretching (above 2800 cm^{-1}) are in this sense much less sensitive. The decrease of the signal as the basis set size increases is rather counterintuitive, as an opposite trend is usual for the static polarizabilities [33]. Clearly, small basis sets overestimate the polarizability changes caused by molecular motions.

The larger basis set spectrum clearly better corresponds to the experimental signal (Figure 2), where a relatively weak signal within 400–1000 cm^{-1} is apparent only if compared to the most distinct H–O–H bending region around 1650 cm^{-1}. We can thus conclude that the simulation of the aqueous Raman scattering using the CPMD approach provides realistic spectrum. A more detailed analysis of the water Raman signal and vibrational properties goes beyond the scope of this work, but can be found in many previous studies [8,34–37].

3.4. Raman spectra of quartz and fused silica

The experimental and calculated quartz and fused silica Raman spectra are presented in Figure 3. The calculated intensity pattern of quartz is in an excellent agreement with the experiment; minor extra peaks in the experiment can be explained by anharmonic interactions (Fermi resonances) and impurities and structural irregularities in the natural crystal. The approach based on the force field diagonalization used in this study seems to provide slightly more realistic crystal band shapes than intensity

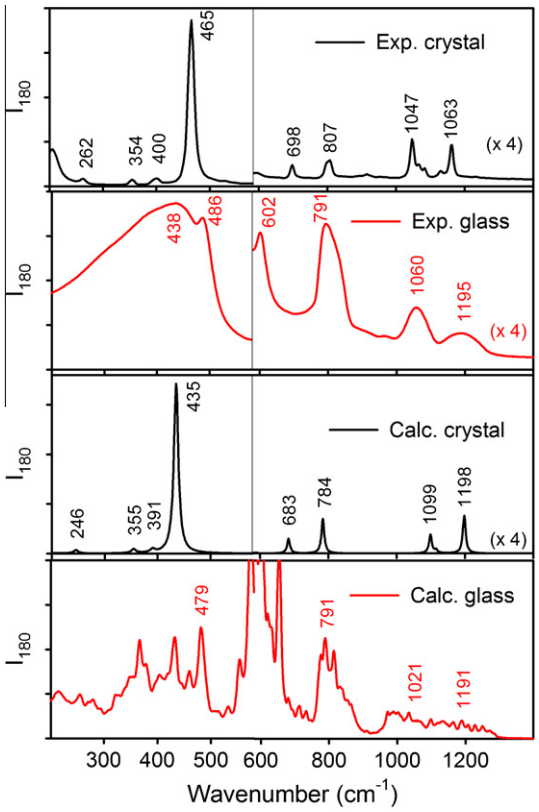

Figure 3. Experimental and calculated backscattered Raman spectra of the crystal (quartz, black line) and fused silica (glass, red) SiO_2 forms. (For interpretation of the references to color in this figure legend, the reader is referred to the web version of this article.)

simulations based on the autocorrelation approach used for a similar mineral previously [14]. In particular, the low-frequency bands are simulated more faithfully.

The correspondence between the calculation and the experiment for fused silica is less obvious; nevertheless the main spectral features can be assigned, as well as the main changes in the spectra accompanying a crystal–glass transition are captured by the theoretical model. For example, the strongest Raman peak in quartz (experimentally at 465 cm^{-1}) disappears in glass, where a broad intense signal appears instead in the whole lowest-frequency (<500 cm^{-1}) region. The calculated spectra of the fused silica glass (Figure 3, bottom) capture this trend; the smooth bandshape, however, was not obtained due to incomplete averaging of the limited number of CPMD configurations. At ~600 cm^{-1}, an increased intensity appears in the experiment. This is reproduced by the

calculation, although the relative intensity is significantly overestimated. Currently, we cannot explain this discrepancy. The sharper experimental band at 486 cm^{-1} can be most probably attributed to the simulated maximum at 479 cm^{-1}. Below this limit the experimental Raman signal is broadened by collective vibrations with a maximum intensity at 438 cm^{-1}, which is only approximately reproduced.

The higher-frequency (>700 cm^{-1}) Raman signal of fused silica is simulated more faithfully. The 807 cm^{-1} quartz experimental band is broadened to a signal centered around 791 cm^{-1}, and well reproduced by the calculation (providing 784 and 791 cm^{-1}, respectively). Also the quartz experimental peaks at 1047 and 1063 cm^{-1} approximately stay at their positions, giving broader bands in fused silica (1060 and 1195 cm^{-1}), which is qualitatively well simulated, except for the incompletely averaged calculated signal.

Interestingly, in the initial stages of optimization a strong band appeared at ~1300 cm^{-1} (not shown) corresponding to a double Si=O bond stretching vibration, which disappeared during the equilibration. This also documents the sensitivity of the Raman signal to the structure, and potential applications of the simulations in material science.

3.5. Contribution of the phonon modes and potential energy distribution

Up to now we calculated the vibrational spectra within the periodic boundary conditions, but only using the $\Gamma(0, 0, 0)$ branch of the crystal modes as implemented in CASTEP. To estimate the error coming from this simplification, namely the neglect of delocalized phonon-like modes in the fused silica glass, we simulated spectra of several adjacent elementary cells ($2 \times 2 \times 2$, $3 \times 3 \times 3$, $4 \times 4 \times 4$) by the FT method based on a propagation in arbitrary time [29] (Figure 4, top). As can be seen, the delocalized phonon-like modes that are possible in the large systems probably cause only insignificant variations of Raman intensities, mostly in the lower-frequency region. In other words, the Raman signal comes mostly from short-range atomic interactions.

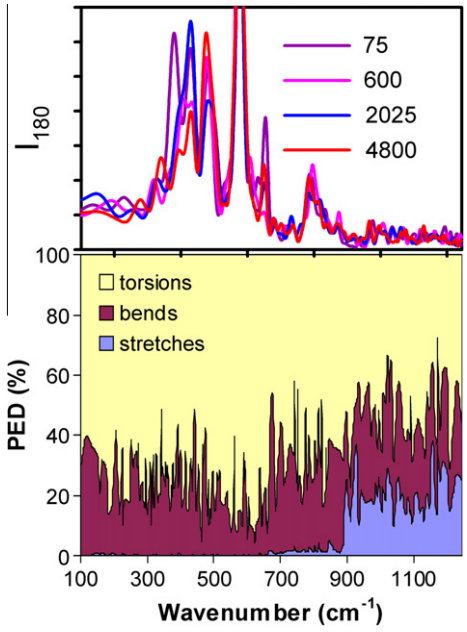

Figure 4. Fused silica Raman spectra simulated by the FT method [29] for different size of a cubic cell (top, number of atoms indicated) and (bottom) decomposition of the vibrational potential energy into individual types of normal modes calculated for one MD geometry in dependence on the vibrational frequency.

The qualitative assignment of fused silica vibrations based on the internal coordinate potential energy distribution (Figure 4, bottom) reveals a different character of the higher-frequency modes (>900 cm^{-1}), containing a substantial part of the Si–O stretching energy. The bending modes (O—Si—O, Si—O—Si) are omnipresent, and so are the torsions. Nevertheless, the minor but still visible contribution of the stretches within 700–900 cm^{-1} suggests that these vibrations are still somewhat similar to the parental vibrations in quartz crystal (cf. Figure 3) and related to the covalent Si—O bonding. Indeed, below this limit, the Raman signal is broadened and cannot be so easily related to that of the quartz.

4. Conclusions

We used the plane wave ab initio MD methodologies and periodic boundary linear response calculations to obtain the geometry, vibrational properties and Raman intensities for the fused silica glass. The model based on a frozen liquid provided geometry parameters that well agreed with the experiment. So did the simulated Raman intensities, although the accuracy was limited, mostly because of the high computational demands of the CPMD simulations. The potential energy distribution analysis indicated a strong contribution of the Si—O stretching to the fused silica vibrations only above ~900 cm^{-1}.

Several aspects of the computational approach were tested also on crystal quartz and liquid water. For crystal quartz, we obtained realistic band shapes and positions, superior to the time-domain approaches reported previously for analogous materials. The water simulations revealed several similarities in the radial and angular distribution functions between the fused silica and liquid water. It also allowed for more extensive testing of the computational procedures. Relatively large basis set was required for accurate calculation of low-frequency Raman signal of liquid water. The ab initio simulations of fused silica Raman spectrum thus provided insight into the amorphous material structure and a valuable link between the spectral and geometrical properties.

Acknowledgement

The study was performed with the support from the Academy of Sciences, Grant Agency of the Czech Republic (P208/11/0105), and the MŠMT (LH11033 and 2B08021). We thank Dr. M. Hušák for his help with the software, and Prof. Vladimír Baumruk for providing us with the water Raman spectrum.

References

[1] J.M. Senior, Optical Fiber Communications, Pearson Education Limited, Harlow, 2009.
[2] J. Bock, G.J. Su, J. Am. Ceram. Soc. 53 (1970) 69.
[3] R.J. Hemley, H.K. Mao, P.M. Bell, B.O. Mysen, Phys. Rev. Lett. 57 (1986) 747.
[4] S.T. Yang, M.J. Matthews, S. Elhadj, D. Cooke, G.M. Guss, V.G. Draggoo, P.J. Wegner, Appl. Optics 49 (2010) 2606.
[5] Y.K. Han, X.W. Lan, T. Wei, H.L. Tsai, H. Xiao, Appl. Phys. A 97 (2009) 721.
[6] H. Aguiar, J. Serra, P. Gonzales, B. Leon, J. Non-Cryst, Solids 355 (2009) 475.
[7] J. Šebestík, P. Bouř, J. Phys. Chem. Lett. 2 (2011) 498.
[8] J. Kapitán, M. Dračínský, J. Kaminský, L. Benda, P. Bouř, J. Phys, Chem. B 114 (2010) 3574.
[9] G.E. Walrafen, P.N. Krishnan, Appl. Optics 21 (1982) 359.
[10] C. Wang, Y. Tamai, N. Kuzuu, J. Non-Cryst, Solids 321 (2003) 204.
[11] M. Klevenz, S. Wetzel, M. Möller, A. Pucci, Appl. Spectrosc. 64 (2010) 298.
[12] G.E. Walrafen, Y.C. Chu, M.S. Hokmabadi, J. Phys. Chem. 94 (1990) 5658.
[13] F.L. Galeener, Phys. Rev. B 19 (1979) 4292.
[14] M. Pagliai, M.M. Miranda, G. Cardini, V. Schettino, J. Mol. Struct. 993 (2011) 151.
[15] R. Car, M. Parrinello, Phys. Rev. Lett. 55 (1985).
[16] B. Kirtman, F.L. Gu, D.M. Bishop, J. Chem. Phys. 113 (2000) 1294.
[17] K. Refson, P.R. Tulip, S.J. Clark, Phys. Rev. B 73 (2006) 155114.
[18] K. Kihara, Eur. J. Miner. 2 (1990) 63.

[19] CASTEP, part of Material Studio, in, Accelrys Software Inc. 2007.
[20] S.J. Clark, M.D. Segall, C.J. Pickard, P.J. Hasnip, M.J. Probert, K. Refson, M.C. Payne, Z. Kristallogr. 220 (2005) 567.
[21] J.P. Perdew, K. Burke, M. Ernzerhof, Phys. Rev. Lett. 77 (1996) 3865.
[22] J. VandeVondele, M. Krack, F. Mohamed, M. Parrinello, T. Chassaing, J. Hutter, Comput. Phys. Commun. 167 (2005) 103.
[23] A. Becke, Phys. Rev. A 38 (1988) 3098.
[24] G. Lippert, J. Hutter, M. Parrinello, Mol. Phys. 92 (1997) 477.
[25] S. Goedecker, M. Teter, J. Hutter, Phys. Rev. B 54 (1996) 1703.
[26] CPMD, in, Max-Planck Institut and IBM Corporation, Stuttgart 2006.
[27] A.D. Becke, J. Chem. Phys. 98 (1993) 5648.
[28] P. Bouř, J. Sopková, L. Bednárová, P. Maloň, T.A. Keiderling, J. Comput. Chem. 18 (1997) 646.
[29] I. Ivani, P. Bouř, J. Chem. Theor. Comput. 6 (2010) 2095.
[30] W.M.M. Haynes, D.R. Lide, CRC Handbook of Chemistry and Physics, NIST, Internet Version 2011, 2011.
[31] R.L. Mozzi, B.E. Warren, J. Appl. Crystallogr. 2 (1969) 164.
[32] J.P. Perdew, Y. Wang, Phys. Rev. B 45 (1992) 13244.
[33] P. Bouř, Chem. Phys. Lett. 265 (1997) 65.
[34] T. Hasegawa, Y. Tanimura, J. Phys, Chem. B 115 (2011) 5545.
[35] H. Torii, J. Phys. Chem. A 110 (2006) 9469.
[36] M. Starzak, M. Mathlouthi, Food Chem. 82 (2003) 3.
[37] M.A. Ricci, G. Signorelli, V. Mazzacurati, J. Phys.: Condens. Matter. 2 (1990) SA183.